
Article:
Gamelon, M. orcid.org/0000-0002-9433-2369, Jenouvrier, S. orcid.org/0000-0003-3324-2383, Lindner, M. orcid.org/0000-0003-2931-265X et al. (2 more authors) (2023) Detecting climate signals cascading through levels of biological organization. Nature Climate Change, 13 (9). pp. 985-989. ISSN 1758-678X

https://doi.org/10.1038/s41558-023-01760-y

Detecting climate signals cascading through levels of biological organization

Marlène Gamelon[1,2], Stéphanie Jenouvrier[3], Melanie Lindner[4,5], Bernt-Erik Sæther[2], Marcel E. Visser[4,5]

[1]Laboratoire de Biométrie et Biologie Evolutive UMR 5558, CNRS, Université Claude Bernard Lyon 1, Villeurbanne, France
[2]Department of Biology, Centre for Biodiversity Dynamics, Norwegian University of Science and Technology, Trondheim, Norway
[3]Biology Department, Woods Hole Oceanographic Institution, Woods Hole
[4]Department of Animal Ecology, Netherlands Institute of Ecology (NIOO-KNAW), P.O. Box 50, 6700 AB Wageningen, the Netherlands
[5]Chronobiology Unit, Groningen Institute for Evolutionary Life Sciences (GELIFES), University of Groningen, Groningen, The Netherlands
* Corresponding author. E-mail: marlene.gamelon@cnrs.fr

Abstract

The time of emergence (ToE) is a novel tool in ecology to detect the threats to a species posed by climate change. It is the time at which the signal of climate change in ecological processes emerges from the noise of ecosystem variability. For the first time, we quantify the ToE in traits, vital rates and population size for a wild species, the great tit (*Parus major*). Using state-of-the-art climate-dependent population models, we predict population dynamics between 1920 and 2100 under climate warming and winter food scenarios. We found that ToE occurred earlier at the level of population size than trait and vital rates, suggesting amplified anthropogenic climate change signal at this level. ToE thus varies across levels of biological organization that filter trends and variability in climate differently, with implications for the detection and attribution of climate impacts on wild species.

The impact of anthropogenic climate change on wildlife populations is a topic of profound concern. Climate change occurs in the context of broad-band natural climate variability, often making it difficult to discern the explicit effects of long-term change driven by forced response to greenhouse gases. In addition, ecological responses to environmental variation are stochastic with multiple sources of variation, including observed and unobserved variability in abiotic and biotic factors that interact with natural climate variability. Accordingly, detecting responses to anthropogenically-forced changes in climate is challenging [1]. This is, however, crucial for the detection and attribution of ecological responses to climate change because changes in climate have direct impacts on ecosystem processes and society [2].

To detect changes in climate, climatologists have extensively used the concept of time of emergence in climate ($ToE_{climate}$) [3,4]. It defines the point in time when the signal of climate change emerges from the noise of natural climate variability. It has been applied for instance on changes in temperatures [3], rainfall [5] and in polar climate [1,4]. Here, we apply this concept, for the first time, across levels of ecological organization to identify the time at which the signal of climate change in ecological processes emerges from the stochastic noise associated with natural climate and ecological variability (time of emergence, ToE). We assess the ToE from trait (ToE_{trait}), to vital rates (e.g. survival, recruitment) (ToE_{vital}), and population size (ToE_{pop}) (Fig. 1) to study how the climate signal cascades through the levels of biological organization. Climate-induced changes in resources, that influence fitness-related traits, are expected to generate changes in vital rates, which lead to population-level responses. We may thus expect that the time of emergence is delayed across levels of biological organization, occurring earlier for traits than for vital rates and population size [6–8]. However, those responses depend on the sensitivity of vital rates to climate variation and the sensitivity of population growth rate to changes in vital rates, potentially driving more complex patterns across levels of biological organization [1,8,9].

There are not many systems for which this hypothesis can be tested because it requires long-term data at various levels of biological organization. Here, we use one of the best long-term ecological time series study system on the great tit (*Parus major*) at the Hoge Veluwe National Park (the Netherlands) from 1985 to 2020 (Fig. 1). The great tit is a short-lived small passerine bird species abundant in European gardens and woodlands and it is not migratory. Global warming influences this population in several ways. In spring, warmer temperatures lead to an advanced peak date of caterpillar biomass, an important food resource for great tits for feeding their offspring during the breeding season. However, the advancement in laying dates is slower than the advancement in food peak date, leading to a phenological mismatch between offspring requirements and food peak [10]. This mismatch influences the vital rates of great tits [11]. In summer, warmer temperatures are expected to influence the intensity and frequency of beechnut production (*Fagus sylvatica*) [12,13], an important food resource for great tits in winter, also affecting their vital rates [14]. Taking advantage of this unique system to quantify the ToE across biological levels of organization, we identified the point in time when climate-driven signals in trait (laying date), vital rates (survival, recruitment) and population dynamics can be distinguished from noise by constructing prediction intervals of ecological projections using the Community Earth System Model Large Ensemble (CESM-LE) [15].

We first quantified the ToE in caterpillar peak dynamics ($ToE_{caterpillar}$). Using the established relationship between spring temperatures and caterpillar peak (period 1985 – 2020)

[16], we projected caterpillar peak dynamics under a high emission climate scenario with no policy intervention (RCP 8.5 scenario), back in the past and into the future, from 1920 to 2100. The peak date of caterpillar biomass advanced over time [16], with an expected $ToE_{caterpillar}$ in 2034, if we only account for climate natural variability (Fig. 2). When many sources of ecological stochasticity were included in the projections, such as uncertainty in parameter estimates and process variance corresponding to unexplained temporal environmental stochasticity beyond that explained by climate, $ToE_{caterpillar}$ was detected later, in 2049 (Fig. S1).

Second, we quantified the ToE in trait dynamics, namely laying date (ToE_{laying}). Using the established relationship between spring temperatures and laying dates (period 1985 – 2020) [16], we projected laying dates dynamics from 1920 to 2100. Laying occurred earlier and earlier over years, with an expected ToE_{laying} in 2045 and 2068 (with climate natural variability only and with all sources of uncertainties, respectively) (Fig. 2, Fig. S1). Under warmer spring conditions, directional selection for earlier laying has been reported in plethora of species [17–24]. The shift in laying date has been interpreted as a phenotypic plastic response to increasing temperatures, tracking the advance in the phenology of the food peak [25–28]. Our results demonstrate that the difference between laying dates and date of the food peak, the so-called phenological mismatch (Fig. 1), might not be detectable before 2100 when including many sources of ecological uncertainties in the projections (Fig. S1). However, when only climate natural variability was accounted for in the modelling, $ToE_{mismatch}$ was detectable and expected to occur in 2049 (Fig. 2). Increasing ecological complexity delays the $ToE_{mismatch}$ as we expected, but mainly through the interaction with environmental stochasticity.

Third, thanks to the individual long-term monitoring of great tits, we estimated annual age-specific great tits vital rates (survival, recruitment) using a state-of-the-art integrated population model [29–32] (period 1985 – 2020, Fig. S2). Annual vital rates were linked to past beechnut production, mismatch and density (period 1985 – 2020, Table S1). Then, we projected age-specific vital rates by 2100 under expected future conditions of mismatch and beechnut production and quantified the ToE in vital rates (ToE_{vital}). Beechnut production is expected to change in the future [33–35], but there is currently no predictive model available for this food resource. Therefore, we simulated two extreme scenarios, one of decreasing beechnut production by 2100 and another of increasing production (Fig. S3). Under the scenario of decreasing beechnut production (scenario 1), we found a decrease in vital rates over time, with a ToE_{vital} between 2050 and 2060 for most of the ages when we only accounted for climate natural variation (Fig. 3, Fig. S4). When all sources of ecological uncertainties were accounted for, ToE_{vital} was not detectable before 2100 (Fig. 3, Fig. S5). Similarly, under the scenario of increasing beechnut production (scenario 2), we found an increase in vital rates over time, with a ToE_{vital} between 2054 and 2084 for most of them when we accounted for climate natural variability only (Fig. 3, Fig. S6). Interestingly, the ToE_{vital} occurred earlier for survival than recruitment rates because of a stronger signal on survival. While the ToE_{vital} did not differ much between the two scenarios for survival, it is delayed up to 20 years for recruitment under the scenario of increasing, compared to decreasing, beechnut production. The climate-driven signals in recruitment rates by beechnut production were obscured by density dependence, which plays a stronger role under favorable conditions (i.e. when there are more years with a high beech crop) and weaker under poor conditions. As expected, when all sources of ecological uncertainties were accounted for, ToE_{vital} was undetectable (Fig. 3, Fig. S7).

Finally, to quantify the ToE in population size (ToE_{pop}), we projected the great tit population size from 1920 to 2100 by parametrizing a stochastic age-structured population model with the projected vital rates (Fig. S4-S7). Under the scenario of decreasing beechnut production, population size decreased with a ToE_{pop} in 2028 when we accounted for climate natural variability only, whereas population size increased under the scenario of increasing beechnut production with a ToE_{pop} in 2055 (Fig. 3). When all sources of ecological uncertainties were accounted for, ToE_{pop} occurred later, in 2069 under the first scenario and in 2074 under the second scenario (Fig. 3).

Remarkably, for any scenario of beech crop production, the ToE_{pop} occurred earlier than the ToE_{vital} when all sources of uncertainties were accounted for. This is consistent with previous work based on numerical simulations that has shown that under a fast rate of environmental change and low predictability, a population can decline before any apparent change in mean value of the trait [8]. Similarly, in an experimental design, a fast change in prey availability resulted in the decline of a protozoan ciliate population preceding a shift in mean body size [8]. Therefore, the ToE_{pop} can occur earlier than ToE_{vital} and the detection of ToE depends on the level of biological organization considered, its sensitivity to climate (i.e. magnitude and shape of the functional relationship between climate and ecological variable), but also on the amount of variability both in the climate and ecological systems.

Climate trends and variability are differently filtered by the vital rates (survival, reproduction) and the ages [1]. In addition, density dependence may prolong the ToE_{pop} [1] as illustrated here with our two scenarios of changes in beech crop production. Under the scenario of decreasing beech crop production (scenario 1), both survival and recruitment rates decrease, the magnitude of this decrease being age-specific. The strength of density dependence also decreases, allowing for more immigrants. The negative influence of beech crop on vital rates, only partially compensated by an increase in the number immigrants, leads to a rapid population decline, with an early ToE. Under the scenario of increasing beech crop production (scenario 2), survival and recruitment rates increase. However, the strength of density dependence also increases, leading to a weak positive effect of beech crop on recruitment rates, the latter being density-regulated [36]. Similarly, the number of immigrants joining the population are positively influenced by beech crop, but strongly regulated by density, resulting in fewer immigrants. The positive influence of beech crop on survival rates, counterbalanced by a strong density regulation acting on the number immigrants and on recruitment rates leads to a moderate increase in population size, and a later ToE_{pop}.

Ecological variability is also key to detect ToE. We found that ToE in mismatch and vital rates are not detectable before 2100 when ecological variability is accounted for, emphasizing the difficulties to detect climate change signals in ecological processes. Thankfully, some of this noise from sampling and process errors can be reduced by increasing monitoring effort and improving our understanding of how the biological systems respond to biotic and abiotic factors.

The detection of ToE across levels of biological organization is context-specific, and the earlier detection at the population level we showed here is unlikely for semelparous species, or if climate affects primarily fertility [1]. In addition, several climate variables with different ToE may affect the various ecological organizational levels, hence making difficult to predict which ecological level may experience an earlier detection of the climate signal. Future studies could

build upon our analysis to better understand and detect when climate-driven changes in ecosystems will clearly emerged from the "noise" of variability across species with contrasting life histories inhabiting different environments (e.g. various climate variability and trends) [1]. This is particularly urgent as ecosystems have a limited ability to adapt, and large changes outside past experience could be particularly devastating [37,38].

Methods

General overview

To detect climate signals cascading through levels of biological organization, we build a reproducible three-step approach (Fig. S8). First, long-term data should be collected from trait values, to vital rates and population size. In parallel, environmental variables should be available. Different methods can be used to estimate annual vital rates and population size when the detection probability is lower than 1, e.g. capture-recapture models or integrated population models (IPM). When the detection probability equals to 1, other methods such as population census or generalized linear models can be used. Second, the effects of environmental covariates on annual variation in trait values, vital rates and population size is assessed. This can be done using linear mixed models (see methods section). Third, these established relationships permit projecting time series of trait values, vital rates and population size under various environmental scenarios in the past and in the future to quantify the time of emergence (Fig. S8) by linking ecological models to dynamic ocean-atmosphere models.

Our methodological approach is divided into several objectives:

(1) Our first objective is to determine the point in time when climate-driven signals in caterpillar peak dates timing can be distinguished from noise ($ToE_{caterpillar}$).
(2) Our second objective is to determine the point in time when climate-driven signals in great tit laying dates can be distinguished from noise (ToE_{laying}).
(3) Our third objective is to determine the point in time when climate-driven signals in mismatch (between laying dates and food peak) can be distinguished from noise ($ToE_{mismatch}$).
(4) Our fourth objective is to determine the point in time when climate-driven signals in vital rates can be distinguished from noise (ToE_{vital} for each age-specific vital rate).
(5) Our fifth objective is to determine the point in time when climate-driven signals in population can be distinguished from noise (ToE_{pop}).

To achieve objectives 1-3, we use functional relationships linking caterpillar peak dates, laying dates and mismatch to temperatures [16]. To achieve objectives 4-5, we built an IPM to estimate annual age-specific vital rates. We then estimated the functional relationships between environmental variables and vital rates using linear mixed models. Finally, to project the great tit population dynamics from 1920 to 2100, we simulated two beech crop production scenarios.

Study site and data collection

The studied population is located at Hoge Veluwe National Park in the Netherlands (*52°02'N, 5°51'E*), a wood of 171 ha. Great tits (*Parus major*) are short-lived small passerine birds, abundant in European gardens and woodlands and, in the Netherlands, not migratory. They are cavity-nesters and readily accept nest boxes as nesting sites, making it possible to monitor the entire breeding population. They produce one or two clutches each year [39]. In the study area, very few females bred in natural cavities and most of them bred in nest boxes [40]. The population is open to immigration and emigration [11].

The data used in this study were collected between 1985 and 2020. Nest boxes were visited during the breeding season and laying dates were recorded (1st egg laid). In addition, three types of demographic data were recorded. First, the total number of breeding females (C_t). As most females start to breed at one year of age, the breeding population size is a good proxy for the total number of females [41]. Second, fledglings were marked with a uniquely numbered leg-ring, ringed mothers identified and unringed mothers given a ring to allow for future identifications. These unringed mothers were assumed to have immigrated into the population during the year in question. The following year, they are then considered to be local females. Overall, 2,204 breeding females of known age (local and immigrant) were monitored, providing capture-recapture (CMR) data of known age females. We grouped the breeding birds of known age into four age classes: 1, corresponding to the first year of breeding (i.e., second calendar year of life); 2, corresponding to the second year of breeding; 3 corresponding to the third year of breeding; and 4, which groups breeding females in their fifth calendar year of life and older. Third, ringed fledglings were recorded as recruited to the breeding population if they were caught breeding in a subsequent year. From the monitoring of breeding females of known age, we reported for each year t the observed number of breeding females in age class i ($B_{i,t}$) and also the observed number of locally recruited females produced per age class i ($J_{i,t}$). In total, this type of demographic data based on reproductive success consisted of 3,675 breeding events.

Environmental data collection: food peak, mismatch, beech crop index and temperatures

Between 1985 and 2020 (except 1991), annual peak dates of caterpillar biomass (hereafter food peak) were determined [42]. The annual mismatch corresponded to the difference in mean laying date for great tits minus the food peak plus 33. These 33 days accounted for incubation duration and assumed that nestlings have the highest energy demand 10 days after hatching [16]. In addition to caterpillars, beech mast is an important food resource for great tits, especially during winter when other resources are scarce. It is also indicative of seed production of other tree species [14,40]. The beech crop index (BCI), measured as the net weight of all nuts per m^2, was recorded annually as a three-level index (1, 2 or 3).

Annual temperatures were recorded. Previous work showed that laying dates in this great tit population depended on spring temperatures from 11 March to 20 April (hereafter $Temp_{laying}$), whereas temperatures from 6 March to 14 May had the strongest influence on food peaks (hereafter $Temp_{caterpillar}$) [16]. We thus recorded annual temperatures during these two time windows. We standardized $Temp_{laying}$ and $Temp_{caterpillar}$ with the mean and the variance of $Temp_{laying}$ and $Temp_{peak}$ observed during this period, so $Temp_{laying}$ and $Temp_{caterpillar}$ were transformed as z-scores. Temperature data were obtained from the De Bilt station of the KNMI (Royal Dutch Meteorological Institute), less than 50 km from the Hoge Veluwe field site.

Objective 1: Forecasting food peak and estimating $ToE_{caterpillar}$

In this population, food peak dates (in Julian date) are linked to temperatures ($Temp_{caterpillar}$) through this relationship [16]:

$$food\ peak = 138.379\ (se: 0.629) - 7.162\ (se: 0.629) \times Temp_{caterpillar} + 3.719 \quad \text{Eqn. 1}$$

From this relationship, we estimated past (1920-2019) and future (2020-2100) food peak dates according to the RCP 8.5 climate scenario that considers no policy intervention. This scenario brings together 40 ensemble members diagnosing the influence of internal climate variability on projections [15]. The mean and the standard deviation over 1985-2020 of all members were used to transform temperatures ($Temp_{caterpillar}$) into z-scores. Thus, the mean and the standard deviation used for standardizing each of the members was the mean of means and the mean of standard deviations calculated for each member. Such a rescaling allowed observed temperatures in the study site and climate scenarios (on average across all 40 of them) to be aligned between 1985 and 2020 so that they had the same mean and variance. From Eqn. 1, we performed 100 simulations, parameters in the equation being drawn from normal distributions. This resulted in 100 simulations per member, that is 4,000 simulations from 1920 to 2100. This gave us expected food peak dates when all sources of ecological uncertainties were accounted for, including parameter uncertainty and process variance corresponding to unexplained temporal variation in parameters beyond that explained by climate.

After having visually controlled for a good match between observed food peak dates and predicted dates (period 1985-2020, Figure 2), we selected an historical time window during which food peak dates were stable over time (1922-1950, slope of the regression between food peak dates and years during this time window: 0.032 (SE: 0.025)). We computed the lower bound ($LB_{caterpillar}$) of the 66% prediction interval for food peak dates during this historical period, and determined the point in time when the upper bound ($UB_{caterpillar}$) of the 66% prediction interval for food peak dates became lower than $LB_{caterpillar}$. This point corresponded to the time of emergence for food peak ($ToE_{caterpillar}$). In addition, we forecasted food peak dates but we only accounted for climate uncertainty in the projections. To do so, we turned off standard errors and σ (the last term) in Eqn. 1 to obtain 40 projections of food peak dates from 1920 to 2100, i.e. one projection per member.

Objective 2: Forecasting laying dates and estimating ToE_{laying} (=ToE_{trait})

We replicated the same procedure for laying dates. In this population, laying dates (in Julian date) are linked to temperatures ($Temp_{laying}$) through this relationship [16]:

$$laying\ date = 110.980\ (se: 0.582) - 4.947\ (se: 0.590) \times Temp_{laying} + 3.493 \quad \text{Eqn. 2}$$

We estimated the expected annual laying dates between 1920 and 2100 according to the RCP 8.5 climate scenario, with all sources of uncertainty, and when only climate uncertainty was accounted for. We selected an historical time window during which laying dates were stable over time (1922-1950, slope of the regression between laying dates and years during this time window: 0.019 (SE: 0.017)), and we identified the time of emergence for laying dates (ToE_{laying}).

Objective 3: Forecasting mismatch and estimating $ToE_{mismatch}$

We then calculated the mismatch between laying dates and food peak from 1920 to 2100 as the difference in expected annual laying dates minus the expected annual food peak plus 33[16]. This was done for the 4,000 simulations accounting for all sources of uncertainties, and for the 40 simulations accounting for climate uncertainty only. In both cases, we identified the time of emergence for mismatch ($ToE_{mismatch}$).

Objectives 4-5: Forecasting vital rates and population dynamics and estimating ToE_{vital} and TOE_{pop}

1- Estimating annual age-specific vital rates and densities

For populations with a recapture rate of 1, population census can be used as a proxy of population size, and survival rates can simply be estimated using generalized linear model with binomial link function, based on whether or not the individual has been observed. Here, we used an integrated population model (IPM) to obtain accurate and precise estimates of annual population size and age-specific vital rates. Even if the recapture probability is high on the study site [11], still not all females may be recaptured, resulting in biased estimates of vital rates and number of individuals. There was also a possibility of double counts, for instance if one female has produced two broods but was only identified in one of them (because she has deserted one of the clutches), and a possibility that some clutches are missed (because females have bred in natural cavities). To estimate age-specific demographic rates and density while accounting for these issues, we integrated the recorded number of breeding females (C_t), CMR data of females of known age, and data on reproductive success (i.e., $B_{i,t}$ and $J_{i,t}$) into an IPM [30] (Figure S2). This framework allowed us to obtain the posterior median of age-specific vital rates (survival $S_{i,t}$, recruitment $R_{i,t}$), the number of local (N_{local}) and immigrant (Nim) breeding females in each age class N_i and in total N (total density) for each year t with improved precision and free of observation error [29–32,43]. The joint analysis of these three datasets thus allowed us to account for observation error associated with the recorded number of counted breeding females [44]. It also allowed us to account for the incomplete information on age structure in the monitoring data (e.g. some females are of unknown age), for imperfect detection (e.g. recapture probability is not 1) and for demographic stochasticity [45].

The likelihood of the IPM corresponds to the product of the likelihoods of the three different datasets, namely CMR data, reproductive success data and population counts [43]. For CMR data of breeding females of known age, we used the Cormack-Jolly-Seber model [46] which allows estimation of annual survival between age class i and $i+1$ ($S_{i,t}$) and annual recapture (p_t) probabilities. For data on reproductive success, the observed number of daughters locally recruited per age class i ($J_{i,t}$) is Poisson distributed with $J_{i,t} \sim \text{Poisson}(B_{i,t} \times R_{i,t})$, where R is the recruitment rate of females of age class i at year t. For the population count data, we used a state-space model [47] that consisted of a process model describing how the population size and structure changed over time as well as an observation model [29]. We considered a pre-breeding age-structured model with the four pre-defined age classes.

The model was fitted within a Bayesian framework using NIMBLE (version 0.9.1) [48]. We ran four independent chains with different starting values for 200,000 MCMC iterations, with a burn-in of 150,000 iterations, thinning every 100th observation and resulting in 2,000 posterior samples. We used the Brooks and Gelman diagnostic $\hat{R}$ to assess the convergence of the simulations and used the rule $\hat{R} < 1.1$ to determine whether convergence was reached [49]. For a full description of the IPM, the priors used and the R code to fit the IPM, see Gamelon et al. [50].

2- Linking vital rates to BCI, mismatch and density

The IPM was used to estimate annual age-specific vital rates and densities. Once these were estimated, we linked annual age-specific vital rates and annual number of immigrants joining the local population as response variables to annual density, BCI and mismatch (from 1985 to 2020) (see life cycle on Fig. 1). The same approach has been done in previous studies [51–53] that first used an IPM to estimate vital rates and density, and then used regressions to link vital rates to density and/or environmental covariates. As the annual vital rates and densities are estimated in the IPM model, they are not obscured by sampling variance and observation errors and thus this approach does not lead to spurious detection of density dependence [50,54,55]. In detail, survival between two successive breeding seasons *t* and *t+1* could be affected by BCI at time *t*. Therefore, we linked age-specific survival rates $S_{i,t}$ (on a logit-scale) to BCI at *t*. Because the effect of BCI on survival may be age-specific, we included the interaction between age and BCI. To account for the non-independence of the survival rates among age classes of a given year, we included the year as a random effect. The linear-mixed model (LMM) took the following form:

$$logit\,(S_{i,t}) = \mu + \beta_{1,i}\,a + \beta_2\,BCI_t + \beta_{3,i}\,[a \times BCI_t] + \beta_{year}\,year + \varepsilon_{S_t} \quad \text{Eqn. 3}$$

where μ is the intercept, *a* is the age class (i.e. 1, 2, 3 and 4), β are the regression coefficients, *year* is the random effect and $\varepsilon_{S_{i,t}}$ corresponds to the residuals of the LMM. Note that the LMM was weighted by the inverse of the variance of the survival rates (on a logit-scale) to account for the uncertainty associated with the survival rates estimated with the IPM.

The recruitment rate of a given breeding season *t* could be affected by the number of breeding females at time *t* in the population (density at *t*) and by BCI at time *t*. Therefore, we linked the age-specific recruitment rates $R_{i,t}$ (on a log-scale) to density at *t* N_t and to BCI at *t.* Because the effect of BCI and density on recruitment may be age-specific, we included the interaction between age and BCI and between age and density. The LMM took the following form:

$$log(R_{i,t}) = \nu + \beta_{1,i}'\,a + \beta_2'\,BCI_t + \beta_3'\,N_t + \beta_{4,i}'\,[a \times BCI_t] + \beta_{5,i}'\,[a \times N_t] + \beta_6'\,year + \varepsilon_{R_{i,t}} \quad \text{Eqn. 4}$$

where ν is the intercept, *a* is the age class, β' are the regression coefficients, and $\varepsilon_{R_{i,t}}$ corresponds to the residuals of the LMM. As done for survival rates, the LMM was weighted by the inverse of the variance of the recruitment rates (on a log-scale) to account for the uncertainty associated with the recruitment rates estimated with the IPM.

The number of immigrants joining the population during the breeding season *t+1* may be influenced by BCI and mismatch as well as the number of local breeding females N_{local} at *t*. Therefore, we linked the number of immigrant breeding females Nim_{t+1} to the number of local breeding females $N_{local,t}$, BCI and mismatch at *t* using a generalized linear model (GLM) with Poisson distribution:

$$Nim_{t+1} = \eta + \beta_{I,1}\,BCI_t + \beta_{I,2}\,Mism_t + \beta_{I,3}\,N_{local,t} + \varepsilon_{I_{t+1}} \quad \text{Eqn. 5}$$

where η is the intercept, β_I are the regression coefficients, and $\varepsilon_{I_{t+1}}$ corresponds to the residuals of the GLM.

3- Building the population model

For given conditions of BCI, mismatch and densities, age-specific survival and recruitment rates as well as the number of immigrants joining the local population may be simulated (hereafter denoted $S_{sim\ i,t}$, $R_{sim\ i,t}$ and $Nim_{sim,t+1}$). As a result, the number of breeding females in the population $N_{sim,t}$ may be simulated.

In detail, the total number of breeding females in the population at time $t+1$ $N_{sim,t+1}$ corresponded to the sum of breeding females in each age class i $N_{sim\ i,t+1}$ at time $t+1$ (Figure 1):

$$N_{sim,t+1} = N_{sim\ 1,t+1} + N_{sim\ 2,t+1} + N_{sim\ 3,t+1} + N_{sim\ 4,t+1} \quad \text{Eqn. 6}$$

(i) As most of the immigrant breeding females were females of age class 1, we assumed that $N_{sim\ 1,t+1}$ corresponded to the sum of the number of daughters that were locally recruited into the population $n_{sim,t+1}$ (i.e. produced by the breeding females of each age class) and also of the number of immigrants $Nim_{sim,t+1}$ arriving into the population:

$$N_{sim\ 1,t+1} = n_{sim,t+1} + Nim_{sim,t+1} \quad \text{Eqn. 7}$$

$n_{sim,t+1}$ was modeled using a Poisson distribution to include demographic stochasticity:

$$n_{sim,t+1} \sim Poisson\left(N_{sim\ 1,t} \times R_{sim\ 1,t}\right) + Poisson\left(N_{sim\ 2,t} \times R_{sim\ 2,t}\right) + Poisson\left(N_{sim\ 3,t} \times R_{sim\ 3,t}\right) + Poisson\left(N_{sim\ 4,t} \times R_{sim\ 4,t}\right) \quad \text{Eqn. 8}$$

(ii) $N_{sim\ 2,t+1}$ corresponded to the number of females of age class 1 that survived from time t to time $t+1$, and was modeled using a binomial process to include demographic stochasticity:

$$N_{sim\ 2,t+1} \sim Bin\left(N_{sim\ 1,t}, S_{sim\ 1,t}\right) \quad \text{Eqn. 9}$$

(iii) $N_{sim\ 3,t+1}$ and $N_{sim\ 4,t+1}$ corresponded to the number of females in the previous age class that survived from time t to time $t+1$:

$$N_{sim\ 3,t+1} \sim Bin\left(N_{sim\ 2,t}, S_{sim\ 2,t}\right) \quad \text{Eqn. 10}$$

$$N_{sim\ 4,t+1} \sim Bin\left(N_{sim\ 3,t}, S_{sim\ 3,t}\right) + Bin\left(N_{sim\ 4,t}, S_{sim\ 4,t}\right) \quad \text{Eqn. 11}$$

Therefore, for given conditions of BCI, mismatch and densities, $S_{sim\ i,t}$, $R_{sim\ i,t}$ and $Nim_{sim,t+1}$ may be computed. We accounted for sources of environmental stochasticity due to processes other than covariates included in the model with a covariance matrix $\mathbf{\Sigma}$ of "random *year* effect + $\varepsilon_{S_{i,t}}$" and "random *year* effect + $\varepsilon_{R_{i,t}}$". The covariance matrix was estimated and new residuals were generated from a multivariate normal distribution with covariance matrix equal to $\mathbf{\Sigma}$. Then, $N_{sim\ 1,t+1}$, $N_{sim\ 2,t+1}$, $N_{sim\ 3,t+1}$ and $N_{sim\ 4,t+1}$, functions of $S_{sim\ i,t}$, $R_{sim\ i,t}$ and $Nim_{sim,t+1}$ may be computed and finally, the density $N_{sim,t+1}$ may be simulated.

4- Forecasting vital rates and population size and estimating ToE_{vital} and ToE_{pop}

Using the age-structured population model described above, that accounted for the effects of BCI, mismatch and density on vital rates, we forecasted the great tit population under two simulated beech crop production scenarios.

a) Forecasting beech crop index under two scenarios

BCI is a categorical variable with three levels (1 (low), 2 (medium) and 3 (high production)). We simulated two extreme scenarios of beech crop production by 2100.

In the first scenario, we simulated a decrease in beech crop production in the future. The probability of having a year of low production (P(BCI=level 1)) increased over time, from 0.005 in1920 to 0.9 in 2100. The probability of having a year of medium production (P(BCI=level 2)) was set to 0.1, the average observed between 1985 and 2020. The probability of having a year of high production (P(BCI=level 3)) corresponded to 1-P(BCI=level 1)-P(BCI=level 2) and thus ranged from 0.895 to 0 from 1920 to 2100 (Fig. S3, left panel). For each year, we performed 100 draws from a three-category multinomial distribution with probabilities P(BCI=level 1), P(BCI=level 2), P(BCI=level 3). This resulted in 100 simulated time-series of BCI between 1920 and 2100. These projections of BCI expressed as levels (1, 2 and 3) were used afterwards to project the great tit population size.

In the second scenario, we simulated an increase in beech crop production in the future. The probability of having a year of high production (P(BCI=level 3)) increased over time, from 0.005 in 1920 to 0.9 in 2100. The probability of having a year of medium production (P(BCI=level 2)) was set to 0.1. The probability of having a year of low production (P(BCI=level 1)) corresponded to 1-P(BCI=level 2)-P(BCI=level 3) and thus ranged from 0.895 to 0 from 1920 to 2100 (Fig. S3, right panel). For each year, we performed 100 draws from a three-category multinomial distribution with probabilities P(BCI=level 1), P(BCI=level 2), P(BCI=level 3). This resulted in 100 simulated time-series of BCI between 1920 and 2100.

b) Forecasting vital rates and great tit population size

Using trajectories of mismatch expected from 1920 to 2100 under the RCP 8.5 scenario that accounted for all sources of uncertainties (see objective 3) and simulated trajectories of BCI simulated according to the first scenario (decreasing beech crop production) as well as the age-specific densities in 1987 estimated with the IPM, we simulated 100 stochastic trajectories in vital rates and population sizes per ensemble member from 1920 to 2100, resulting in a total of 4,000 stochastic trajectories. We computed the 95% and 66% prediction intervals of the predicted age-specific vital rates, number of immigrants and total population size. We then selected an historical time window during which population size was stable over time (1922 – 1950, slope of the regression between population size and years during this time window: 0.092 (SE: 0.217)) and estimated the time of emergence for population size (ToE_{pop}) and vital rates (ToE_{vital}). In addition, we forecasted the great tit population but accounted for climate uncertainty only in the projections. To do so, we used trajectories of mismatch expected from 1920 to 2100 that accounted for climate uncertainty only, and turned off stochasticity in Eqn. 8-11 as well as the covariance matrix, to obtain 40 projections of age-specific vital rates and population sizes from 1920 to 2100, i.e. one projection per member.

We replicated the exact same procedure with trajectories of BCI simulated according to the second scenario (increasing beech crop production) to obtain forecasted time-series of vital rates and population size.

All of these analyses were performed with R software [56].

Data and code availability: All data, code, and materials used in the analysis are available at https://github.com/ToEgreattit/data-code

Ethics: The research was carried out under licence AVD801002017831 of the Centrale Commissie Dierexperimenten (CCD) in the Netherlands. Fieldwork at the National Park de Hoge Veluwe was carried out with permission of the Park.

References:

1. Jenouvrier, S. *et al.* Detecting climate signals in populations across life histories. *Glob. Change Biol.* **28**, 2236–2258 (2022).
2. Malhi, Y. *et al.* Climate change and ecosystems: threats, opportunities and solutions. *Philos. Trans. R. Soc. B Biol. Sci.* **375**, 20190104 (2020).
3. Mahlstein, I., Knutti, R., Solomon, S. & Portmann, R. W. Early onset of significant local warming in low latitude countries. *Environ. Res. Lett.* **6**, 034009 (2011).
4. Landrum, L. & Holland, M. M. Extremes become routine in an emerging new Arctic. *Nat. Clim. Change* **10**, 1108–1115 (2020).
5. Rojas, M., Lambert, F., Ramirez-Villegas, J. & Challinor, A. J. Emergence of robust precipitation changes across crop production areas in the 21st century. *Proc. Natl. Acad. Sci.* **116**, 6673–6678 (2019).
6. Clements, C. F., Blanchard, J. L., Nash, K. L., Hindell, M. A. & Ozgul, A. Body size shifts and early warning signals precede the historic collapse of whale stocks. *Nat. Ecol. Evol.* **1**, 1–6 (2017).
7. Clements, C. F. & Ozgul, A. Including trait-based early warning signals helps predict population collapse. *Nat. Commun.* **7**, 10984 (2016).
8. Baruah, G., Clements, C. F., Guillaume, F. & Ozgul, A. When Do Shifts in Trait Dynamics Precede Population Declines? *Am. Nat.* **193**, 633–644 (2019).
9. Hilde, C., H. *et al.* The demographic buffering hypothesis: evidence and challenges. *Trends Ecol. Evol.* **35**, 523–538 (2020).
10. Visser, M. E., Noordwijk, A. J. van, Tinbergen, J. M. & Lessells, C. M. Warmer springs lead to mistimed reproduction in great tits (Parus major). *Proc. R. Soc. Lond. B Biol. Sci.* **265**, 1867–1870 (1998).
11. Reed, T. E., Jenouvrier, S. & Visser, M. E. Phenological mismatch strongly affects individual fitness but not population demography in a woodland passerine. *J. Anim. Ecol.* **82**, 131–144 (2013).
12. Övergaard, R., Gemmel, P. & Karlsson, M. Effects of weather conditions on mast year frequency in beech (Fagus sylvatica L.) in Sweden. *For. Int. J. For. Res.* **80**, 555–565 (2007).
13. Nussbaumer, A. *et al.* Patterns of mast fruiting of common beech, sessile and common oak, Norway spruce and Scots pine in Central and Northern Europe. *For. Ecol. Manag.* **363**, 237–251 (2016).
14. Perdeck, A. C., Visser, M. E. & Van Balen, J. H. Great tit *Parus major* survival and the beech-crop cycle. *Ardea* **88**, 99–106 (2000).
15. Kay, J. E. *et al.* The Community Earth System Model (CESM) Large Ensemble Project: a community resource for studying climate change in the presence of internal climate variability. *Bull. Am. Meteorol. Soc.* **96**, 1333–1349 (2015).
16. Visser, M. E., Lindner, M., Gienapp, P., Long, M. C. & Jenouvrier, S. Recent natural variability in global warming weakened phenological mismatch and selection on seasonal timing in great tits (Parus major). *Proc. R. Soc. B Biol. Sci.* **288**, 20211337 (2021).

17. Both, C. & Visser, M. E. Adjustment to climate change is constrained by arrival date in a long-distance migrant bird. *Nature* **411**, 296–298 (2001).
18. Porlier, M. *et al.* Variation in phenotypic plasticity and selection patterns in blue tit breeding time: between- and within-population comparisons. *J. Anim. Ecol.* **81**, 1041–1051 (2012).
19. Reed, T. E., Jenouvrier, S. & Visser, M. E. Phenological mismatch strongly affects individual fitness but not population demography in a woodland passerine. *J. Anim. Ecol.* **82**, 131–144 (2013).
20. Gamelon, M. *et al.* Environmental drivers of varying selective optima in a small passerine: a multivariate, multiepisodic approach. *Evolution* **72**, 2325–2342 (2018).
21. Marrot, P., Charmantier, A., Blondel, J. & Garant, D. Current spring warming as a driver of selection on reproductive timing in a wild passerine. *J. Anim. Ecol.* **87**, 754–764 (2018).
22. Le Vaillant, J., Potti, J., Camacho, C., Canal, D. & Martínez-Padilla, J. Fluctuating selection driven by global and local climatic conditions leads to stasis in breeding time in a migratory bird. *J. Evol. Biol.* **34**, 1541–1553 (2021).
23. Vatka, E., Orell, M., Rytkönen, S. & Merilä, J. Effects of ambient temperatures on evolutionary potential of reproductive timing in boreal passerines. *J. Anim. Ecol.* **90**, 367–375 (2021).
24. Sæther, B.-E., Engen, S., Gustafsson, L., Grøtan, V. & Vriend, S. J. G. Density-dependent adaptive topography in a small passerine bird, the collared flycatcher. *Am. Nat.* **197**, 93–110 (2021).
25. Charmantier, A. *et al.* Adaptive phenotypic plasticity in response to climate change in a wild bird population. *Science* **320**, 800–804 (2008).
26. Matthysen, E., Adriaensen, F. & Dhondt, A. A. Multiple responses to increasing spring temperatures in the breeding cycle of blue and great tits (*Cyanistes caeruleus*, *Parus major*). *Glob. Change Biol.* **17**, 1–16 (2011).
27. Charmantier, A. & Gienapp, P. Climate change and timing of avian breeding and migration: evolutionary versus plastic changes. *Evol. Appl.* **7**, 15–28 (2014).
28. Villemereuil, P. de *et al.* Fluctuating optimum and temporally variable selection on breeding date in birds and mammals. *Proc. Natl. Acad. Sci.* **117**, 31969–31978 (2020).
29. Besbeas, P., Freeman, S. N., Morgan, B. J. T. & Catchpole, E. A. Integrating mark-recapture-recovery and census data to estimate animal abundance and demographic parameters. *Biometrics* **58**, 540–547 (2002).
30. Schaub, M. & Abadi, F. Integrated population models: a novel analysis framework for deeper insights into population dynamics. *J. Ornithol.* **152**, 227–237 (2011).
31. Brooks, S. P., King, R. & Morgan, B. J. T. A Bayesian Approach to Combining Animal Abundance and Demographic Data. *Anim. Biodivers. Conserv.* **27**, 515–529 (2004).
32. Schaub, M. & Kéry, M. *Integrated population models: Theory and ecological applications with R and JAGS.* (Elsevier Science, 2021).
33. Drobyshev, I., Niklasson, M., Mazerolle, M. J. & Bergeron, Y. Reconstruction of a 253-year long mast record of European beech reveals its association with large scale temperature variability and no long-term trend in mast frequencies. *Agric. For. Meteorol.* **192–193**, 9–17 (2014).
34. Bogdziewicz, M., Kelly, D., Thomas, P. A., Lageard, J. G. A. & Hacket-Pain, A. Climate warming disrupts mast seeding and its fitness benefits in European beech. *Nat. Plants* **6**, 88–94 (2020).

35. Bogdziewicz, M. *et al.* Climate warming causes mast seeding to break down by reducing sensitivity to weather cues. *Glob. Change Biol.* **27**, 1952–1961 (2021).
36. Reed, T. E., Grøtan, V., Jenouvrier, S., Sæther, B.-E. & Visser, M. E. Population growth in a wild bird is buffered against phenological mismatch. *Science* **340**, 488–491 (2013).
37. Beaumont, L. J. *et al.* Impacts of climate change on the world's most exceptional ecoregions. *Proc. Natl. Acad. Sci.* **108**, 2306–2311 (2011).
38. Hawkins, E. *et al.* Observed emergence of the climate change signal: from the familiar to the unknown. *Geophys. Res. Lett.* **47**, (2020).
39. Husby, A., Kruuk, L. E. B. & Visser, M. E. Decline in the frequency and benefits of multiple brooding in great tits as a consequence of a changing environment. *Proc. R. Soc. B Biol. Sci.* **276**, 1845–1854 (2009).
40. Grøtan, V. *et al.* Spatial and temporal variation in the relative contribution of density dependence, climate variation and migration to fluctuations in the size of great tit populations. *J. Anim. Ecol.* **78**, 447–459 (2009).
41. Dhondt, A. A., Adriaensen, F., Matthysen, E. & Kempenaers, B. Nonadaptive clutch sizes in tits. *Nature* **348**, 723–725 (1990).
42. Ramakers, J. J. C., Gienapp, P. & Visser, M. E. Comparing two measures of phenological synchrony in a predator–prey interaction: Simpler works better. *J. Anim. Ecol.* **89**, 745–756 (2020).
43. Kéry, M. & Schaub, M. *Bayesian Population Analysis using WinBUGS: A hierarchical perspective*. (Academic Press, 2012).
44. Lebreton, J.-D. & Gimenez, O. Detecting and estimating density dependence in wildlife populations. *J. Wildl. Manag.* **77**, 12–23 (2013).
45. Lande, R. *et al.* Estimating density dependence from population time series using demographic theory and life-history data. *Am. Nat.* **159**, 321–337 (2002).
46. Lebreton, J.-D., Burnham, K. P., Clobert, J. & Anderson, D. R. Modeling survival and testing biological hypotheses using marked animals: a unified approach with case studies. *Ecol. Monogr.* **62**, 67–118 (1992).
47. de Valpine, P. & Hastings, A. Fitting population models incorporating process noise and observation error. *Ecol. Monogr.* **72**, 57–76 (2002).
48. Valpine, P. de *et al.* Programming With Models: Writing Statistical Algorithms for General Model Structures With NIMBLE. *J. Comput. Graph. Stat.* **26**, 403–413 (2017).
49. Brooks, S. P. & Gelman, A. General methods for monitoring convergence of iterative simulations. *J. Comput. Graph. Stat.* **7**, 434–455 (1998).
50. Gamelon, M. *et al.* Density dependence in an age-structured population of great tits: identifying the critical age classes. *Ecology* **97**, 2479–2490 (2016).
51. Hansen, B. B. *et al.* More frequent extreme climate events stabilize reindeer population dynamics. *Nat. Commun.* **10**, 1616 (2019).
52. Abadi, F. *et al.* Estimating the strength of density dependence in the presence of observation errors using integrated population models. *Ecol. Model.* **242**, 1–9 (2012).
53. Gamelon, M. *et al.* Interactions between demography and environmental effects are important determinants of population dynamics. *Sci. Adv.* **3**, e1602298 (2017).
54. Freckleton, R. P., Watkinson, A. R., Green, R. E. & Sutherland, W. J. Census error and the detection of density dependence. *J. Anim. Ecol.* **75**, 837–851 (2006).
55. Schaub, M., Jakober, H. & Stauber, W. Strong contribution of immigration to local population regulation: evidence from a migratory passerine. *Ecology* **94**, 1828–1838 (2013).

611 56. R Development Core Team. R: A language and environment for statistical computing.
612 (2017).
613

614 **Acknowledgements:** We are grateful to all those who have collected data and Louis
615 Vernooij and Judith Risse for maintaining the long-term great tit database. We thank the board of
616 the National Park of Hoge Veluwe for permission to carry out our research in their Park. This
617 work was supported by the Research Council of Norway through its Centres of Excellence
618 funding scheme, project number 223257, and by the CNRS.

Figures

Fig. 1. Schematic illustration of the general approach. The first panel shows forecasted caterpillar peak dates, great tit laying dates, mismatch between caterpillar peak date and laying date, as well as beech crop production (two scenarios) in the studied great tit population expected from 1920 to 2100. From the ecological time series, the points in time when climate-driven signals in food peak, laying and mismatch can be distinguished from noise (ToE) are identified. On the second panel, great tit life cycle showing age-specific vital rates (survival S_i, recruitment R_i) and the number of immigrants joining the population (*Nim*) as functions of mismatch, beech crop and density *N*. On the third panel, forecasted vital rates and great tit population size from 1920 to 2100 according to expected mismatch under global warming and beech crop (two scenarios). From the time series of vital rates and population sizes, the points in time when climate-driven signals in vital rates (ToE_{vital}) and population size (ToE_{pop}) can be distinguished from noise are identified.

Fig. 2. Caterpillar peak dates, great tit laying dates, and mismatch forecasted under global warming in the studied great tit population between 1920 and 2100. Each line corresponds to one climate scenario (40 in total), and the black line corresponds to the mean. Vertical dotted lines indicate the historical period (1922-1950), horizontal line indicates the lower bound of the 66% interval during that period. Vertical red line corresponds to the time of emergence (ToE). In thick blue, annual observed values between 1985 and 2020.

Fig. 3. Times of Emergence (ToE) from caterpillar peak dates to population size in the Hoge Veluwe great tit population. Columns show the ToE for the two scenarios of beech crop production (scenario 1: decreasing production by 2100; scenario 2: increasing production) for the different levels of biological organization (in rows). In red, ToE when only climate uncertainty is accounted for, and in grey ToE when all sources of ecological uncertainties are accounted for.

647 Figure 1

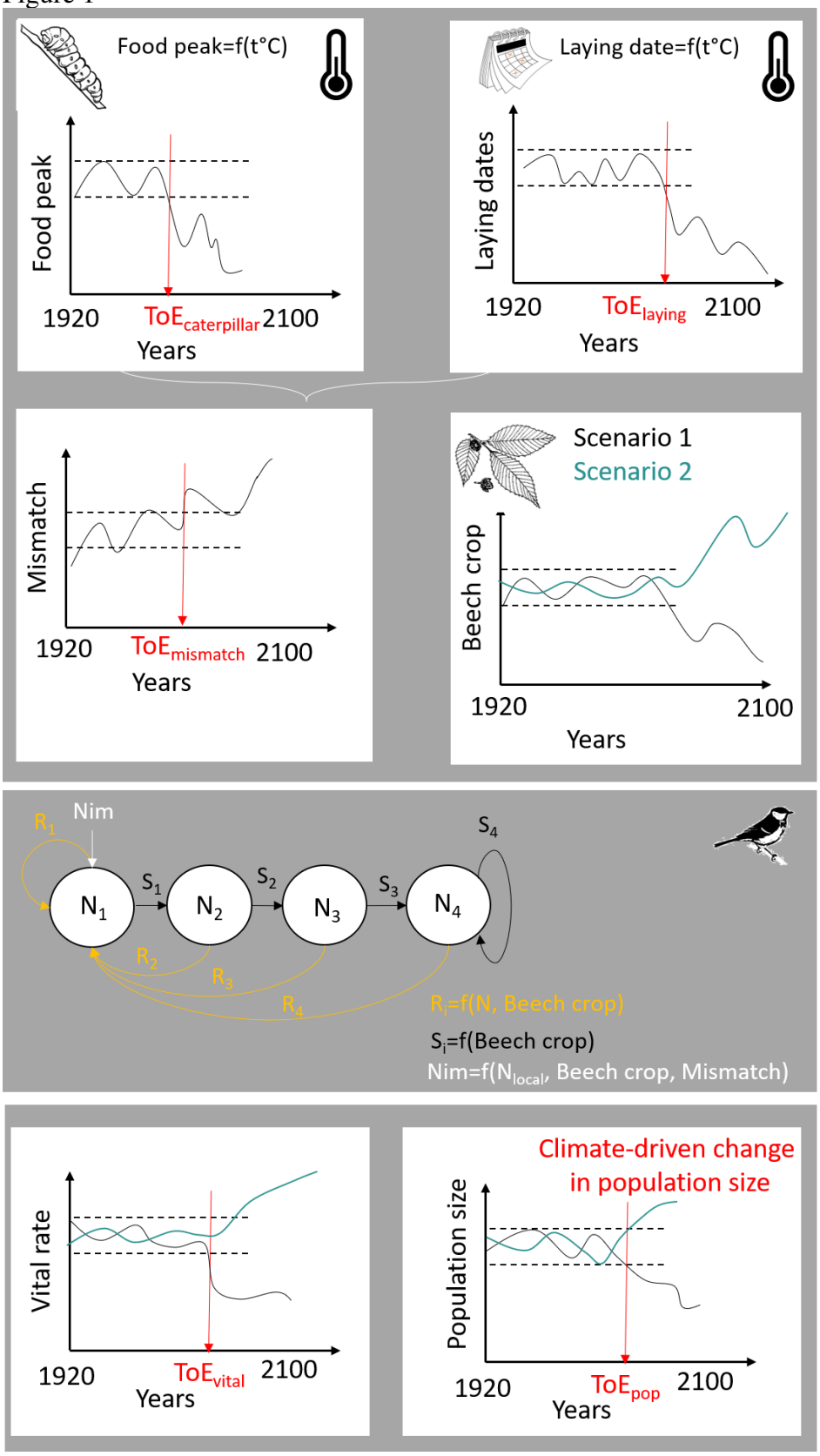

648
649

650 Figure 2

651

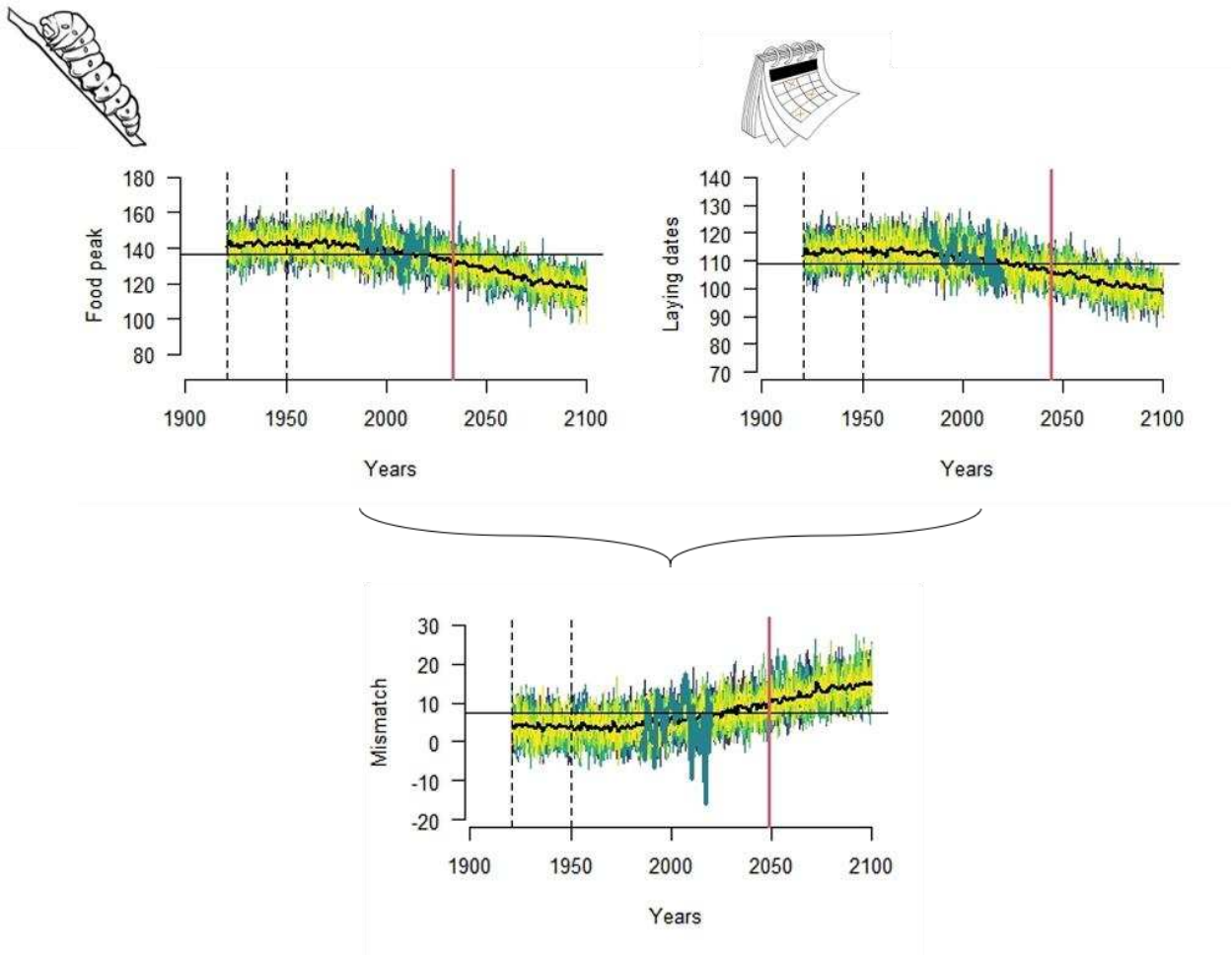

652
653

654

655 Figure 3
656

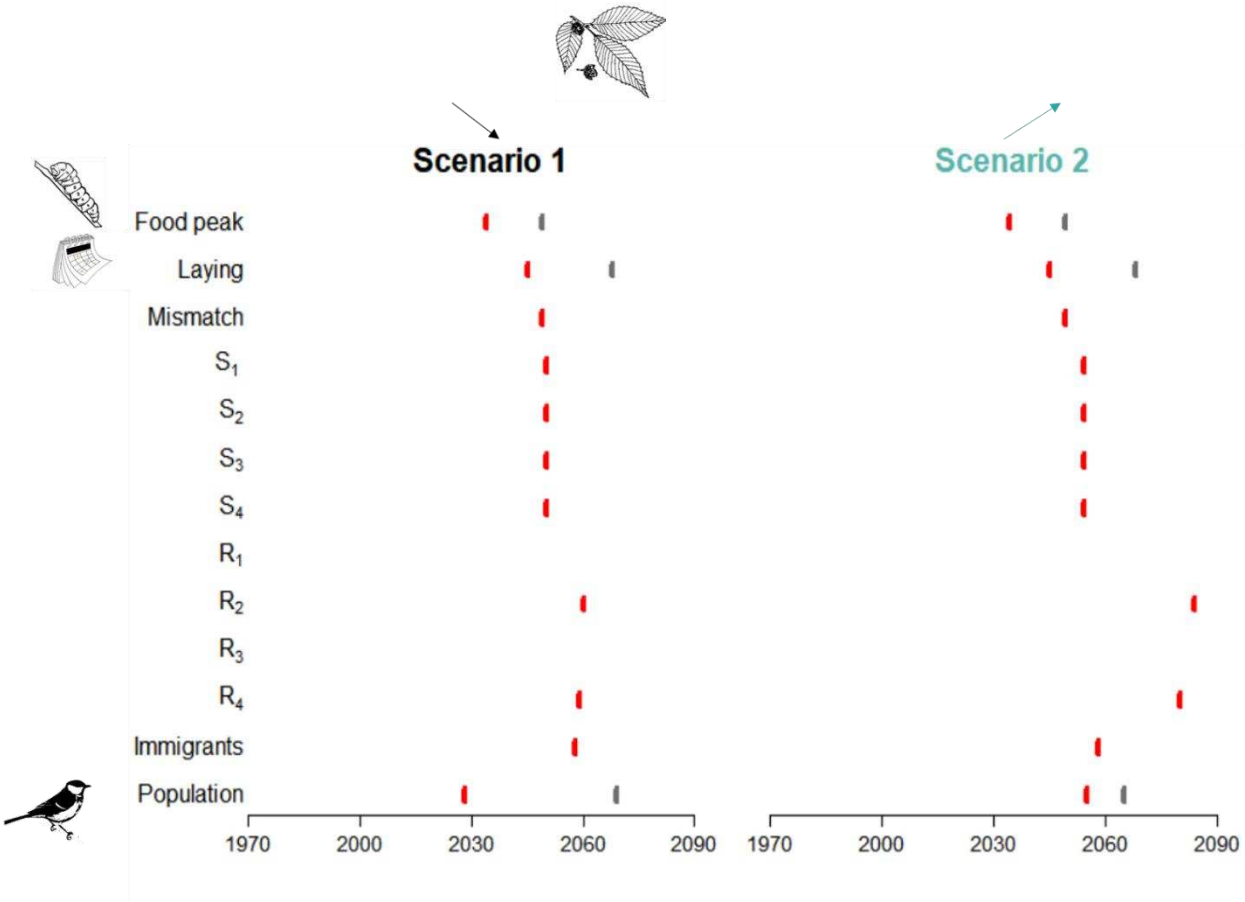

657
658